Advanced Composite Materials
Publication details, including instructions for authors and subscription information:
http://www.tandfonline.com/loi/tacm20

Numerical Simulation of Mechanical Behavior of Composite Structures by Supercomputing Technology

Seung Jo Kim [a], Kuk Hyun Ji [b] & Seung Hoon Paik [c]

[a] Flight Vehicle Research Center, Seoul National University, Seoul, Korea, School of Mechanical and Aerospace Engineering, Seoul National University, San 56-1, Shillim-dong, Kwanak-gu, 151-742, Seoul, Korea;, Email: sjkim@snu.ac.kr

[b] School of Mechanical and Aerospace Engineering, Seoul National University, San 56-1, Shillim-dong, Kwanak-gu, 151-742, Seoul, Korea

[c] School of Mechanical and Aerospace Engineering, Seoul National University, San 56-1, Shillim-dong, Kwanak-gu, 151-742, Seoul, Korea

Version of record first published: 02 Apr 2012.

VSP

Advanced Composite Materials 17 (2008) 373–407

ADVANCED COMPOSITE MATERIALS
www.brill.nl/acm

Numerical Simulation of Mechanical Behavior of Composite Structures by Supercomputing Technology

Seung Jo Kim [a,b,*], **Kuk Hyun Ji** [b] **and Seung Hoon Paik** [b]

[a] Flight Vehicle Research Center, Seoul National University, Seoul, Korea
[b] School of Mechanical and Aerospace Engineering, Seoul National University, San 56-1, Shillim-dong, Kwanak-gu, 151-742, Seoul, Korea

Received 27 August 2008; accepted 27 August 2008

Abstract

This paper will examine the possibilities of the virtual tests of composite structures by simulating mechanical behaviors by using supercomputing technologies, which have now become easily available and powerful but relatively inexpensive. We will describe mainly the applications of large-scale finite element analysis using the direct numerical simulation (DNS), which describes composite material properties considering individual constituent properties. DNS approach is based on the full microscopic concepts, which can provide detailed information about the local interaction between the constituents and micro-failure mechanisms by separate modeling of each constituent. Various composite materials such as metal matrix composites (MMCs), active fiber composites (AFCs), boron/epoxy cross-ply laminates and 3-D orthogonal woven composites are selected as verification examples of DNS. The effective elastic moduli and impact structural characteristics of the composites are determined using the DNS models. These DNS models can also give the global and local information about deformations and influences of high local in-plane and interlaminar stresses induced by transverse impact loading at a microscopic level inside the materials. Furthermore, the multi-scale models based on DNS concepts considering microscopic and macroscopic structures simultaneously are also developed and a numerical low-velocity impact simulation is performed using these multi-scale DNS models. Through these various applications of DNS models, it can be shown that the DNS approach can provide insights of various structural behaviors of composite structures.

Keywords

DNS, finite elements, laminates, woven composites, high performance computing

1. Introduction

Composite materials are used today in a variety of industries, and the study of their behavior is assuming increased importance. Combinations of different materials result in superior mechanical characteristics and make it possible to overcome several

* To whom correspondence should be addressed. E-mail: sjkim@snu.ac.kr
Edited by the KSCM

DOI:10.1163/156855108X385339

technical barriers. They have a number of advantages over conventional materials: high specific strength and stiffness, good fatigue performance and corrosion resistance. But, since composite materials are obviously heterogeneous at the constituent material level, their structural behavior may be complicated, which is the main reason that the modeling and simulation of composite materials is important. The precise modeling and accurate simulation of composite materials have been essential for a fundamental understanding and a prediction of the performance of a variety of composite structures. The recognition of these basic needs along with the ever increasing computing power has established computer modeling approaches as one of the major areas in composite materials research because modeling simulation of composite materials plays a key role in understanding and predicting structural behavior of composite structures.

A number of methods that are relevant to the computational modeling and simulation of composite materials have been presented in order to solve the problems related to composite structures. They are conveniently classified into two broad categories: micro-mechanics and macro-mechanics. The micro-mechanic approach is the study of composite material behavior wherein the interaction of the constituent materials is examined on a microscopic scale. The macro-mechanic approach is the study of composite material behavior wherein the material is presumed homogeneous and the effects of the constituent materials are detected only as averaged apparent properties of the composite. The micro-mechanical approach is preferred for an accurate description and prediction of cracking or delamination at the constituent level. In these failure analyses of composite materials, a very fine modeling with micro-mechanics is required, which leads to very large sets of computation. Moreover, the enormous amount of data generated from computer simulations would itself require massive computing power and a comprehensive modeling strategy. Therefore, we need to consider a modeling strategy for composite material systems that focuses on the multi-scale and multi-physics nature of emergent problem areas in composite materials.

Computation is now a crucial part of most basic science and engineering disciplines. This has been facilitated by the astounding growth in computing power over the last two decades, in conjunction with the refinement and expansion of simulation algorithms. Computers combine the best aspects of mechanical models with the ability to process vast amounts of data, and are therefore excellent tools for testing our understanding of the complex nature of materials, often providing new insights. Using current computing technology we are now able to model most physical situations on a very fine scale or multi-scale. Ideas can be accurately simulated before committing expensive resources to experimental equipment. Advances in computer hardware and parallel computing techniques have now made possible engineering analysis of large-scale microscopic analysis that were previously not within the reach of computational resources.

The key aspect of this paper is the direct numerical simulation (DNS) of the composite material for analysis using a large scale, parallel configuration compu-

tation. It has been realized that very large scale and high performance computing may be the key to unlocking many of the complex problems facing composite material analysis. Using DNS, material characterization and structural behaviors such as low-velocity impact of metal matrix composite (MMC) laminates and 3-D orthogonal woven composites are presented, respectively, in this paper. The parallel processing technique has been recognized as the key technology for dealing with large-scale simulations in a reasonable computation time.

2. Direct Numerical Simulation of Composite Materials

The current numerical analysis of laminated composite structures can be grouped into the following two approaches: macroscopic and microscopic [1, 2]. In the macroscopic approaches, composite materials are assumed to be a continuum with homogenized materials properties based on orthotropic or anisotropic constitutive equations. Because the effects of the constituent materials are considered only as averaged apparent properties of the composite, internal stress description inside the material is difficult in the macroscopic approaches. Pagano and Yuan [3] reported the defect of the homogenization scheme for prediction of detailed failure characteristics of composites. It is well known that a failure caused by an impact loading is attributed to the micro-level stresses in the constituents, which are responsible for the failure initiation process in composites since the composite failure always originates from the micro-scale. Consequently, the macroscopic approach is inadequate for evaluation of local stress and prediction of failure, because the behaviors of constituents cannot be described in terms of homogenized material properties.

Because some approaches based on the classical laminate theory had limits in obtaining accurately the interface stresses, many studies have sought to overcome this lack. Layerwise theories [4] were developed by assuming that displacement fields through the thickness of a laminate are only C° continuous functions of the out-of-plane coordinate. This assumption allows for discontinuous transverse strains and, consequently, continuous transverse stresses at the interfaces between layers made of different materials. A displacement field can vary in a layerwise manner through the thickness of the laminate thus allowing for zig-zag variations of the in-plane displacements just as they occur in actual laminated composites. But, this approach has also some intrinsic limitations in describing the local behaviors at the level of the constituents inside composite structures. Though layerwise theory can be applied to obtain interlaminar stress accurately at the level of the ply, detailed full 3-D stress states cannot be obtained at the level of constituents. Since interlaminar cracks were known as the main causes of delamination originated from inside of the constituents such as the matrix, the microscopic approach should be considered for accurate prediction of impact damages.

On the other hand, in the microscopic approaches such as using the unit cell [5] and representative volume element [6], composite laminates are regarded as mixtures of different isotropic or anisotropic materials, and the constituents of

composite materials are modeled separately. The advantage of the microscopic representation is that detailed information is directly obtained about the local interaction between the constituents and micro-failure mechanisms [7]. The microscopic mechanical model, however, has been restricted to the effective mechanical moduli prediction of a continuous fiber-reinforced lamina in terms of the corresponding material properties, relative volume contents, and geometric arrangements of the fiber and matrix materials. The unit cell method assumes that the reinforcements are distributed regularly within the matrix, and laminates are represented by a periodic unit cell in the three-dimensional space. Basically, the unit cell method reduces the size of the problem to one unit cell by imposing constraints in the spatial arrangement of the reinforcements, and the overall composite response can be obtained from the behavior of the three-dimensional unit cell with periodic boundary conditions.

However, there are limits in the domain range that the unit cell method can cover in a microscopic approach. It should be noted that this approach is rather another methodology for homogenization since it assumes identical states and that the periodic reinforcement distribution for all of the unit cells and the damages due to impact events are restricted to a local area. Macroscopic properties of laminated composites may be also influenced by the elastic properties and fiber orientation in each laminate layer. Cumulative damage events, i.e., ply cracks, at the lamina-microscopic scale can also influence mechanical behavior and failure at the macroscopic laminate scale. Thus, traditional microscopic approach such as unit cell method also has difficulties in applying directly to dynamic simulation such as impact events. Moreover, it is clear that a microscopic approach alone will not explain the failure process of the laminates simply because the mutual interaction between the micro-stresses and interlaminar stress in the failure process has been totally neglected.

In the direct numerical simulation (DNS) approach [8–10], we directly discretize the whole composite structures through separate modeling of fiber and matrix at the microscopic level for the 3-dimensional analysis. Figure 1 shows a cross-section micrograph and the finite element DNS model of boron/aluminum laminates. The DNS models describe directly the micro-structures as presented in Fig. 1a. DNS

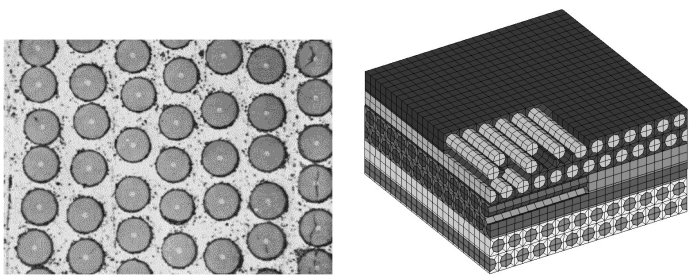

(a) (b)

Figure 1. (a) A micrograph of a cross-section of MMC, (b) DNS finite element model.

uses 3-dimensional solid finite elements since they do not employ the shell assumptions. Instead they utilize a general three-dimensional continuum description, which intuitively seems reasonable since a shell or plate structure in reality is a solid structure. Furthermore, since there is no artificial assumption of displacement or stress through the thickness, DNS can obtain directly distribution of interlaminar stress without specific assumption as long as they have enough finite discretization through the thickness. Especially, the DNS model can obtain directly a detailed description of the 3-D stress state inside the material as against averaged values from the homogenized model. The DNS model can also consider the effect of inhomogeneity by simple and direct manipulation of material properties at the level of the constituents. For analysis and prediction of the impact behaviors of real composite structures, it is required to assess how appropriate the numerical models incorporating full microscopic structures are because the impact-induced behavior and damage are initiated at the microscopic level and propagated to the macroscopic level. Kim *et al.* [10] showed that the DNS model can be used to predict effective elastic moduli of the laminates by the appropriate virtual numerical simulation such as tensile or shear tests using full microscopic DNS model and they concluded that they have a good agreement with Sun and Vaidya's real test results [6]. These results give validation to the fact that DNS model can simulate the real structure. Thus, we can investigate the complex behaviors under impact loading in the fiber–matrix interfaces using the DNS model.

The microscopic studies of the impact on laminates have rarely been conducted yet because they need a huge computing resource and have some difficulties in handling such large-scale data. Though presently existing approaches have been well capable of treating the macroscopic problem, the damage initiation or coupled interactions with the heterogeneous micro-structural details still remains to be adequately settled. As mentioned above, the detailed and more realistic impact analysis at the microscopic level considering the micro-structure inside the materials is essential to the accurate prediction and simulation of impact damage. At the micro-scale, the initial damage modes in the laminates are mostly in the form of micro-cracks that develop throughout fiber, matrix material and/or the matrix–fiber interfaces. The micro-mechanical analysis has the advantage of providing detailed information about these local constituents as well as the interactions among them. This information has been previously lost in the homogenization process used at the macro-scale of laminate analysis. As needs for high precision analysis and safe design are increased, more detailed modeling may be required. Moreover, most failure mechanisms are initiated from microscopic level and a detail modeling incorporating microscopic structure becomes to be necessary. From this point of view, it is meaningful to prospect the future of analysis and design in composite structures that a microscopic modeling and its direct numerical simulation deal with.

Though the DNS approach can obtain detailed information about dynamic behaviors due to the impact events on composite laminates, this methodology requires a large amount of computation resources due to direct modeling of the whole lam-

inates structures at the microscopic level. However, as recent progress of computer technology provides an efficient, effective and low-cost computing performance continuously, the scale of the number of degrees of freedom required in the DNS computation can be extended to the level of more than tens of millions. Thus, it is practicable to make the maximum use of the current computer performance for the accurate DNS analysis. For this reason, we used Pegasus parallel cluster supercomputer system [11] which is composed of 520 processor nodes.

3. Material Characterization

3.1. Laminated MMC

A DNS model is employed to obtain the effective material properties of the metal matrix composite (MMC) laminates. A boron/aluminum composite laminate is selected among possible MMCs for this work. MMCs are being proposed for increased use in structures that require strength at elevated temperatures, damage tolerant behavior and high performance-to-weight ratios. Especially, boron-reinforced aluminum laminates combine the outstanding strength, stiffness and low density of the boron fiber with fabrication and engineering reliability of an aluminum alloy. However, ductile failure by the growth and coalescence of micro-cracks are known to be a dominant failure process in MMCs [12–14]. Fang *et al.* [13] and Aghdam *et al.* [14] showed that using cell, micro-mechanics and finite elements, they predicted effective elastic moduli, elastoplastic stress–strain behaviors and yield and collapse behaviors of MMCs. In the present study, the unit cell model is developed to enable the microscopic modeling inside the material and a whole model of laminated plate is created as the DNS model as a way of assembling unit cells and constructing the structures.

A boron–aluminum MMC laminate consists of rows of boron fibers embedded in a matrix of aluminum. The material properties of boron and aluminum are presented in Table 1. The finite element meshes of the whole laminated plate and its unit cell model are presented along with the coordinate system in Fig. 2. The unit cell model is composed of 16 solid elements for the matrix and 24 solid elements for fibers. The boron fiber and aluminum matrix are assumed to be elastic and isotropic in the DNS model. Virtual experiments for determining material constants of boron–

Table 1.
Material properties for metal matrix composites

Elastic constants	E_1 (GPa)	E_2 (GPa)	G_{12} (GPa)	G_{23} (GPa)	ν_{12}	ν_{23}	Density (g/cm^3)
Fiber (boron)	379.3	379.3	172.41	172.41	0.1	0.1	2.5
Matrix (aluminum)	68.3	68.3	26.27	26.27	0.3	0.3	2.7
Homogenized model	215	134	54.0	51.7	0.20	0.32	2.606

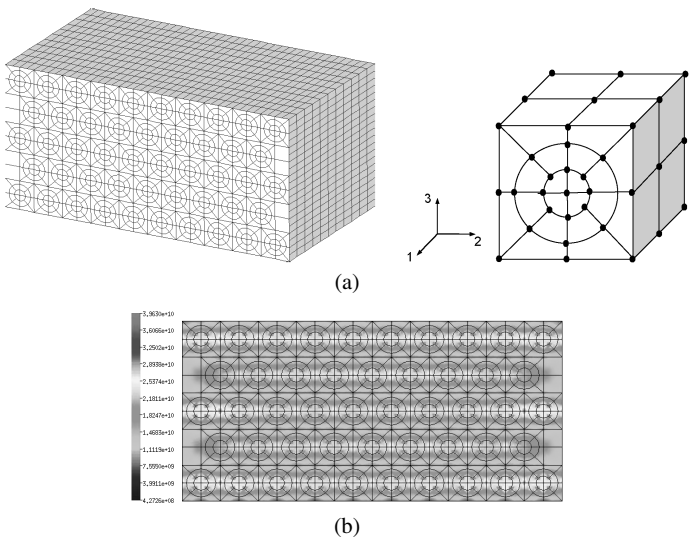

Figure 2. DNS model for MMC laminates: (a) FE model and unit cell, (b) normal stress (σ_{22}) distribution.

Table 2.
Elastic moduli for boron–aluminum composite ($V_f = 0.47$)

Elastic constants (GPa)	Square array [6]	DNS aquare array [10]	Hexagonal array [6]	DNS hexagonal array [10]	The rule of mixture [15]	Elasticity model CCA [16]	Real experiment [12]
E_1	215	215	215	215	214	215	216
E_2	144	143	137	134	130	–	140
G_{12}	57.2	54.3	54.0	54.0	43.7	54.1	52.0
G_{23}	45.9	46.3	52.5	51.7	–	–	–
ν_{12}	0.19	0.20	0.19	0.20	0.21	0.19	0.29
ν_{23}	0.29	0.25	0.34	0.32	–	–	–

aluminum MMC laminates are performed with a DNS model having 0.3 million d.o.f.s. A virtual tensile numerical test for longitudinal modulus, transverse modulus and Poisson ratio are performed and a virtual shear numerical test for shear modulus is performed. In this test, displacement load is applied to the one side and a clamped boundary condition is imposed in the other side. The predicted results show good agreement with real experiments as shown in Table 2 and the normal stress distribution is shown in Fig. 2.

3.2. Active Fiber Composites

An active fiber composite (AFC) is composed of many different materials such as piezoelectric fiber, polymer matrix, kapton mold, electrode and it is usually embedded into glass fiber composites. Figure 3 shows a cross-section and top view of a

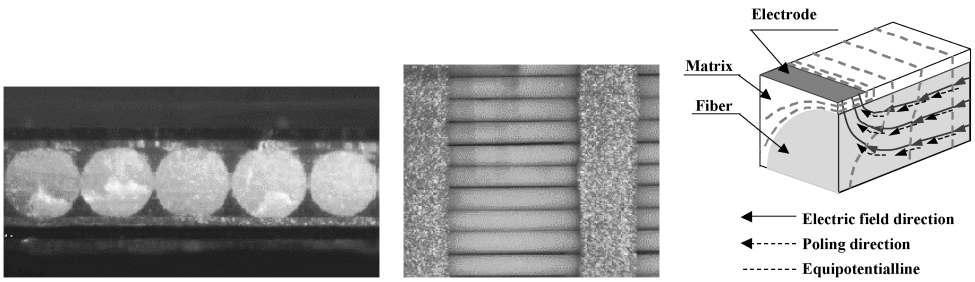

Figure 3. (a) Cross-section, (b) top view [24] and (c) elongation mechanism of AFC [23].

typical AFC and electrode. It is actuated by elongation of active ceramic fiber as demonstrated in Fig. 3c. Piezoelectric fibers are divided into active and inactive regions by an interdigitated electrode (IDE) pattern. For this reason, the arrangement of fibers may not be treated in a regular pattern. In addition, no fibers are embedded in the side edge of an AFC pack. Therefore, it is necessary to adopt a full microscopic model and analyze directly the AFC without repeated boundary or loading assumptions. Some research efforts are addressed in the local stress analysis of AFC through the DNS by the same author [15]. In this section, FE meshing strategy and mechanical material characterization of the AFC pack are discussed.

3.2.1. FE Formulation

FE formulation of a linear static analysis is presented in equation (1) by using the principle of virtual work and a linear elastic constitutive law. If we consider the actuation only, the piezoelectric constitutive relation can be represented as follows:

$$\left(\int \mathbf{B}^{\mathrm{T}}\mathbf{C}\mathbf{B}\,\mathrm{d}V\right)U = \int \mathbf{N}^{\mathrm{T}}\mathbf{p}\,\mathrm{d}S + \int \mathbf{N}^{\mathrm{T}}\mathbf{f}\,\mathrm{d}V, \tag{1}$$

$$\boldsymbol{\sigma} = \mathbf{C}(\boldsymbol{\varepsilon} - \mathbf{d}\mathbf{E}), \qquad \mathbf{E} = \frac{\mathbf{V}}{t}, \tag{2}$$

$$\mathbf{d} = \begin{bmatrix} 0 & 0 & d_{31} \\ 0 & 0 & d_{32} \\ 0 & 0 & d_{33} \\ 0 & d_{24} & 0 \\ d_{15} & 0 & 0 \\ 0 & 0 & 0 \end{bmatrix}, \tag{3}$$

where **B** is the the strain–displacement matrix, **C** is the stress–strain matrix, **U** is the displacement matrix, **N** is the interpolation vector, **p** is the surface traction vector, **f** is the body force vector, $\boldsymbol{\sigma}$ is the stress vector, $\boldsymbol{\varepsilon}$ is the strain vector, **E** is te electric field vector, **V** is peak to peak voltage (V_{pp}), **t** is the distance between the electrode fingers and **d** is the piezoelectric strain tensor.

3.2.2. Modeling of AFC Packs

Figure 4 shows the schematic section view of an AFC pack which was studied to characterize the material properties and actuation performances [16]. As shown in this figure, an AFC consists of a fiber, polymer matrix, kapton mold and kapton substrate and it is embedded in [0°/90°] E-glass composites. The material properties of [0°/90°] E-glass composites are averaged and treated as isotropic material. The other constituents can be treated as isotropic and their Young's moduli are listed in the same reference. The Poisson's ratio is selected as 0.3 for an active fiber and 0.33 for the other constituents. Regarding the coupling coefficients of PZT-5A fiber, $d_{31} = d_{32} = -171 \times 10^{-12}$ C/N and $d_{33} = 374 \times 10^{-12}$ C/N, respectively.

In Figs 5 and 6, the FE mesh of overall and separated view of AFC pack is shown. An edge area in the AFC pack does not exhibit a repeatable mechanical and electrical behavior, as shown in Figs 4 and 6. Since 12 fibers (18%) among the 66 fibers are located out of the electrode coverage, these fibers are not elongated by an electric field. Therefore these fibers should be modeled separately and different attributes are assigned. Interdigitated electrodes with a silver-printed coating on the kapton substrate do not affect the mechanical properties much of the whole AFC pack, so these are not included in the FE model. However, due to the repeated electrode fingers, there are repeated active and inactive regions along the fiber. These two regions are divided and only active regions are compelled to be elongated by

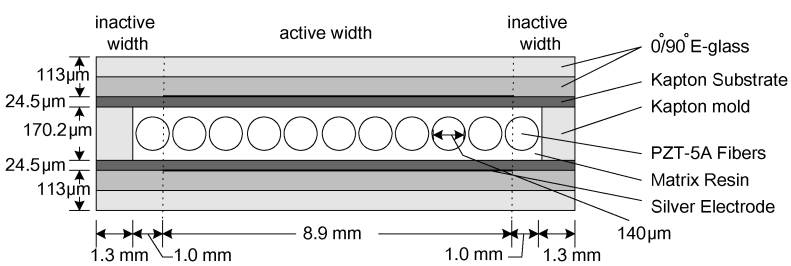

Figure 4. Cross-section of the AFC model of 0°/90° E-glass laminated [18].

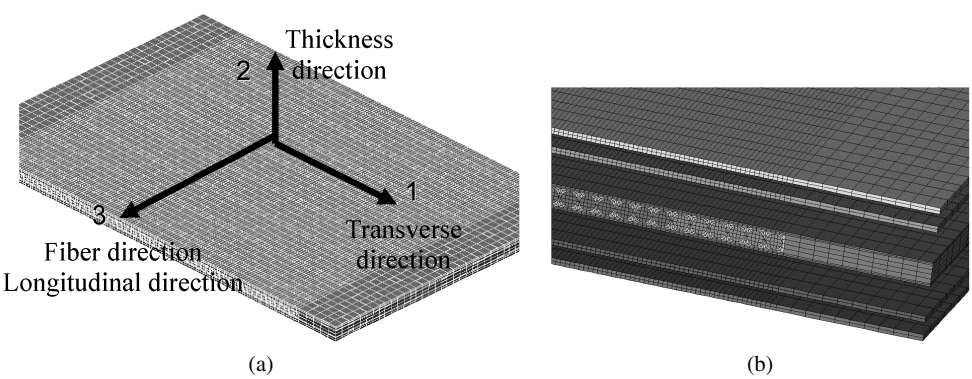

Figure 5. (a) Overall and (b) separated view of AFC pack FE model.

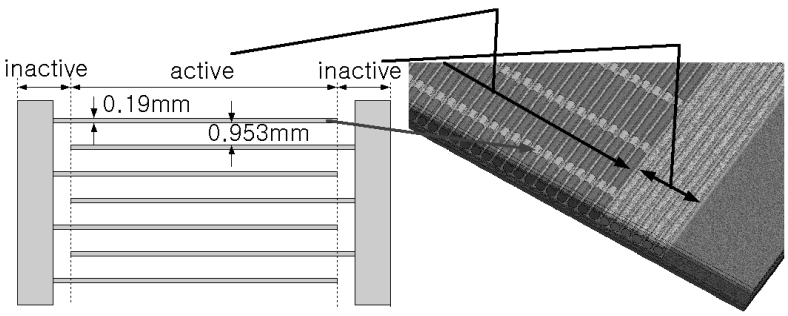

Figure 6. Interdigitated electrode pattern and its location [17].

Table 3.
Comparison of material properties (0°/90° E-glass laminated AFC)

(Unit: GPa)	E_{11}	E_{22}	E_{33}	ν_{12}	ν_{23}	ν_{31}	G_{12}	G_{23}	G_{31}
Experiment [18]	–	–	22.6	–	–	–	–	–	–
Rule of mixture	–	–	22.27	–	–	–	–	–	–
DNS	14.54	9.42	22.09	0.34	0.14	0.33	2.28	3.00	5.42

the electric field. An 8-node solid element is used and the total number of d.o.f. is about 0.8 million.

3.2.3. Mechanical Properties and Local Stress Distribution

In Table 3, the material properties obtained from experiments, rule of mixture and DNS are compared. As can be seen, the predicted results are very close to experimental and analytical results within 1%. Moreover, 3-dimensional material properties can be obtained successfully by DNS. They are difficult to determine experimentally but they are required in 3-D stress analysis for complex structures.

The longitudinal stress distribution of DNS model and averaged model are compared in Fig. 7. The averaged model is one in which material properties of active fiber and polymer are averaged by the rule of mixture. In the averaged model, the averaged fiber–matrix layer exhibits much greater load than the E-glass composites layers, but the differences of load maintained by each of them are relatively small. In the DNS model, however, the longitudinal stress in the fiber region is approximately 30 times larger than that in matrix region. When the stress in the DNS model is compared to that in the averaged model, the stress in the fiber region is three times larger than that in the averaged model; but the stress in the matrix in the averaged model is 10 times larger than that in the DNS model.

3.3. Orthogonal Woven Composites

The DNS model applied to the architecture of yarn geometries in 3-D orthogonal woven composite material is developed in this work. The 3-D orthogonal woven

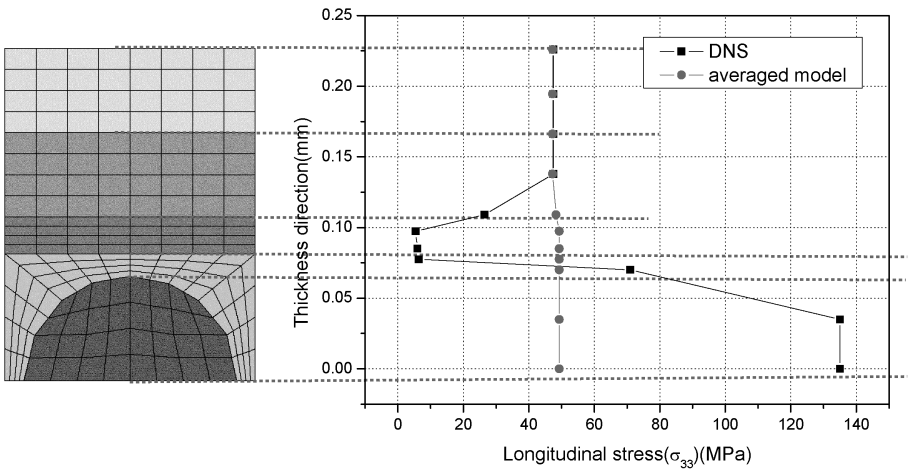

Figure 7. Through thickness normal stress distribution in DNS and averaged model [17].

Table 4.
Material properties of each yarn and matrix [23]

	E_L (GPa)	E_T ($=E_Z$) (GPa)	G_{LT} ($=G_{LZ}$) (GPa)	G_{TZ} (GPa)	ν_{LT} ($=\nu_{LZ}$)	ν_{TZ}	Volume fraction (%)	Density (g/cm^3)
Matrix (epoxy)	2.2	2.2	0.815	0.815	0.35	0.35	39.5	1.16
Fiber (T300)	220	13.8	11.35	5.5	0.2	0.25	–	1.76

composite material is preformed using Torayca T-300(3K) carbon fiber, and then infused with the Epicote 828 epoxy resin (Table 4). Figure 8 depicts the micrographs of the cross-sections cut through the thickness. As can be seen from Fig. 8, there are five layers in the stuffer yarn (x-direction) and six layers in the filler yarn (y-direction). These 11 layers of yarn are interlaced together by the through-the-thickness z-yarn or the warp weaver. The nominal proportions of the stuffer yarn, the filler yarn and the z-yarn are 1:1.2:0.2, respectively, and the overall fiber volume fraction is 0.43.

The procedure for determining the elastic properties of a whole plate for the homogenized model begins with the properties of each yarn. Using the elastic constants of the constituents and the micro-mechanics equations proposed by Chamis [17], the elastic constants for stuffer yarns, filler yarns and z-yarns were calculated [18]. These obtained properties of each yarn were considered to be transversely isotropic since the distribution of the fibers in any two directions normal to a given axis is equivalent in the yarn itself. Then, as a result of the manufacturing process, the 3-D orthogonal woven composite panels have an important feature, namely, existence of a repeating unit structure. The unit structure can be extracted

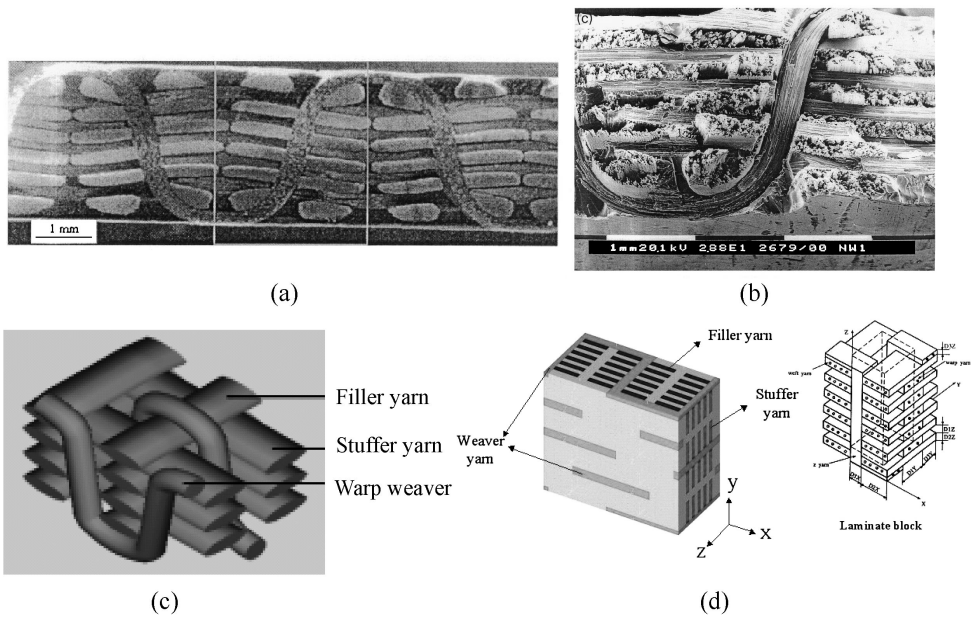

Figure 8. (a) A micrograph of the cross-section for a specimen [22], (b) micrograph of the cross-section (magnified) [22], (c) a schematic model of specimen and (d) unit structure and laminate block [23, 24].

from the material pattern as shown in Fig. 8. Considering the geometry configuration of yarns and matrix, we developed the unit structure which consists of stuffer yarns, filler yarns, weaver yarns and resin. Its schematic view is presented in Figs 9 and 10. The unit structure is modeled by assembling 11,520 brick elements with 8-nodes and it has 13,200 nodes. It is of rectangular type (5.44 × 6.28 mm) with a thickness of 2.79 mm.

The numerical finite element model of the 3-D orthogonal woven composite plate studied here is constructed by assembling some unit structures in x-, y- and z-directions repeatedly to use in material characterization of a whole plate. Since the mechanical properties and geometrical parameters for all the composite constituents are known, the global effective mechanical properties can be determined from results of the material characterization process, such as numerical tensile and pure shear test by DNS approach with high performance computing [19]. According to the material characterization in the reference [20], the virtual numerical tensile and shear test were performed. For the modeling of 3-D orthogonal woven composites, the unit structure is defined and a composite specimen is modeled through rearranging the unit structure in x-, y- and z-direction. For the tensile test, 108 ($27 \times 4 \times 1$) unit structures are used and the total degrees of freedom is 2,671,534; 48 ($12 \times 4 \times 1$) unit structures are used for the shear test. In the shear case, the total degrees of freedom is 1,789,488. From the results of virtual experiments, there is a good agreement between the material properties predicted by virtual character-

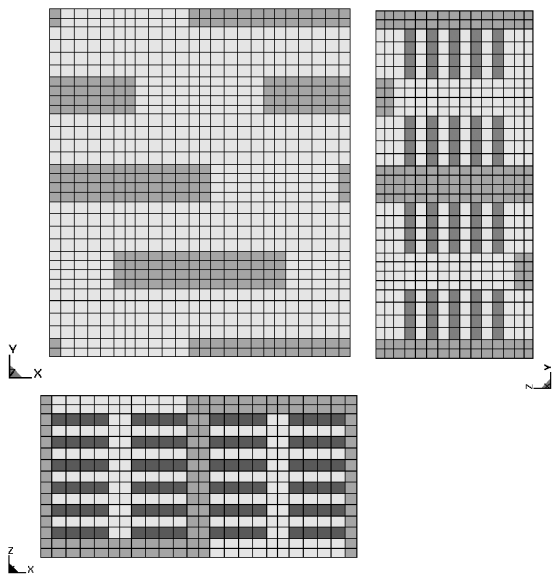

Figure 9. 3-side figure of a unit structure.

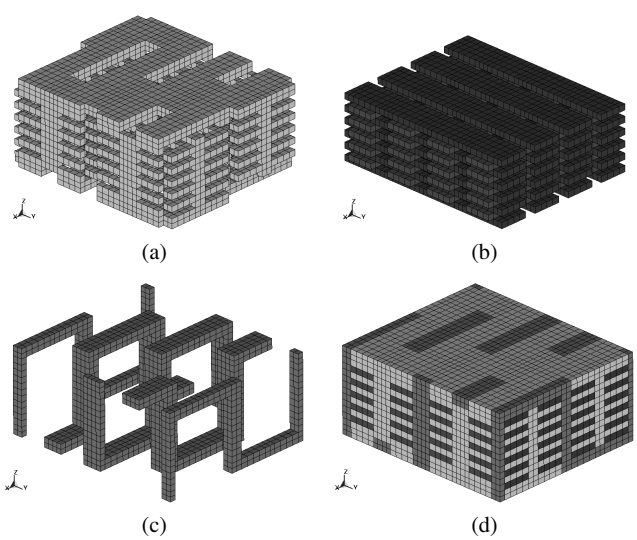

Figure 10. (a) Matrix, (b) stuffer (x) and filler yarn (y), (c) warp weaver and (d) unit structure.

ization and experimental results (Figs 11 and 12, Table 5). But these results may include an overestimate for Young's modulus predicted using the unit cell modeling approach. The difference between the measured and predicted results is less than 0.9% for the longitudinal Young's modulus (i.e., the Young's modulus in the x-direction), 3.5% for the transverse Young's modulus (i.e., the Young's modulus in the y-direction) and 5.4% in plane for the in-plane Poisson's ratio.

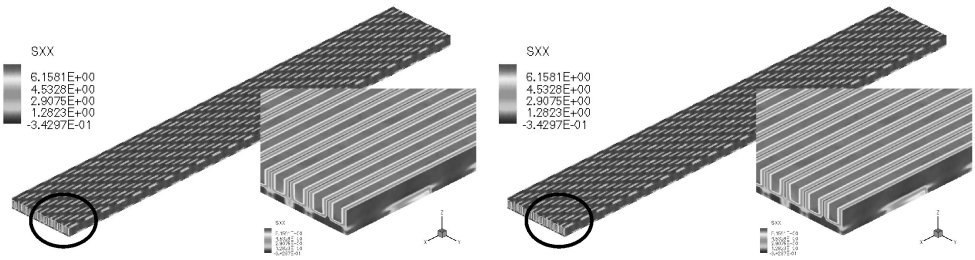

(a) (b)

Figure 11. Results of pure tensile test for E_1: (a) e_{11} distributions, (b) σ_{11} distributions.

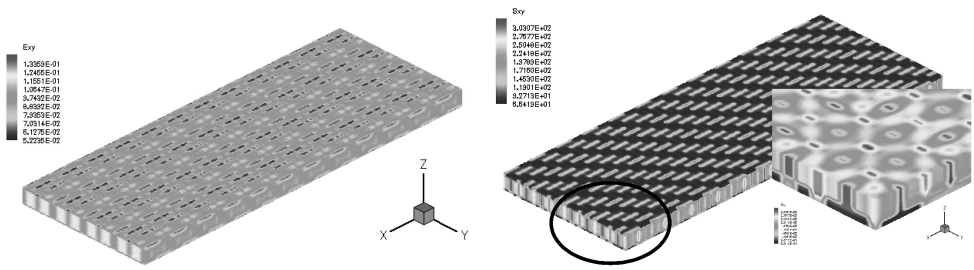

(a) (b)

Figure 12. Results of pure shear test for G_{12}: (a) e_{12} distributions, (b) σ_{12} distributions.

Table 5.
Elastic moduli for 3-D orthogonal woven composites

		E_1 (GPa)	E_2 (GPa)	E_3 (GPa)	ν_{12}	ν_{13}	ν_{23}	G_{12} (GPa)	G_{23} (GPa)	G_{13} (GPa)
Unit cell [5]	XYZ	52.53	59.88	14.53	0.032	0.156	0.155	1.838	2.233	2.289
	YXZ	52.62	59.79	14.53	0.032	0.157	0.154	1.840	2.127	2.389
	ZXY	52.84	60.44	14.00	0.034	0.159	0.162	2.521	2.052	1.925
	ZYX	52.92	60.38	14.00	0.034	0.160	0.161	2.521	1.877	2.085
	FEA	52.76	60.25	14.00	0.034	0.161	0.163	2.558	2.263	2.243
Real experiment [5]		40.97	47.30	–	0.035	–	–	–	–	–
Virtual experiments		40.63	49.00	8.27	0.037	0.34	0.30	2.18	1.97	2.24

The effect of inconsistent spacing of filler yarn on in-plane shear modulus is investigated through virtual characterization. The in-plane shear modulus obtained from inconsistent filler yarn spacing model is 4.22 GPa while the in-plane shear modulus obtained from original consistent model is 2.17 GPa. The stiffness knockdown of 3-D woven composites caused by filler yarn waviness is simulated by virtual characterization. There is about 36% reduction on transverse Young's modulus. From these results, the virtual material characterization of composite materials

can be used for replacing the experimental approaches and designing the 3-D complex composite structures.

4. Structural Behaviors and DNS

4.1. Active Fiber Composites Behavior

One of the main advantages of the DNS approach is that it solves global behaviors and local stresses at the same time with one model. In this section, the feasibility of DNS is verified by comparing elongation measured by experiment under electric field with that from the DNS. A few works in the literature provide actuation results along with the material properties of each constituent. The references for experiment data, material properties and FE model are the same as those used in the material characterization of AFC in the previous section. In this analysis, electric voltage from 500 to 2000 V_{pp} is applied only in the active region of fiber under the free strain condition. Figure 13 represents longitudinal actuation performance of AFC depending on the voltage applied. As shown in this figure, actuation performances obtained from DNS show good agreement with the experiments.

Comparison of the transverse actuation of the laminated actuator obtained from the DNS is presented with the experiment in Table 6. Transverse actuation ratio is

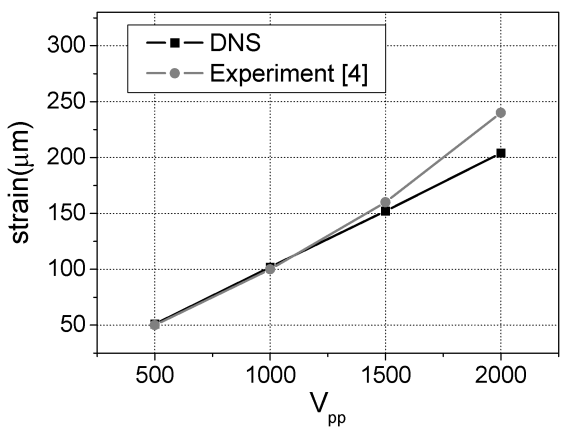

Figure 13. Actuator performance of AFC depending on the voltage variation.

Table 6.
Comparison of transverse actuation ratio of laminated/unlaminated AFC under 2,000 V_{pp}

	DNS [17]	Experiment [18]
Laminated AFC	0.37	0.38
Unlaminated AFC	0.43	Not available

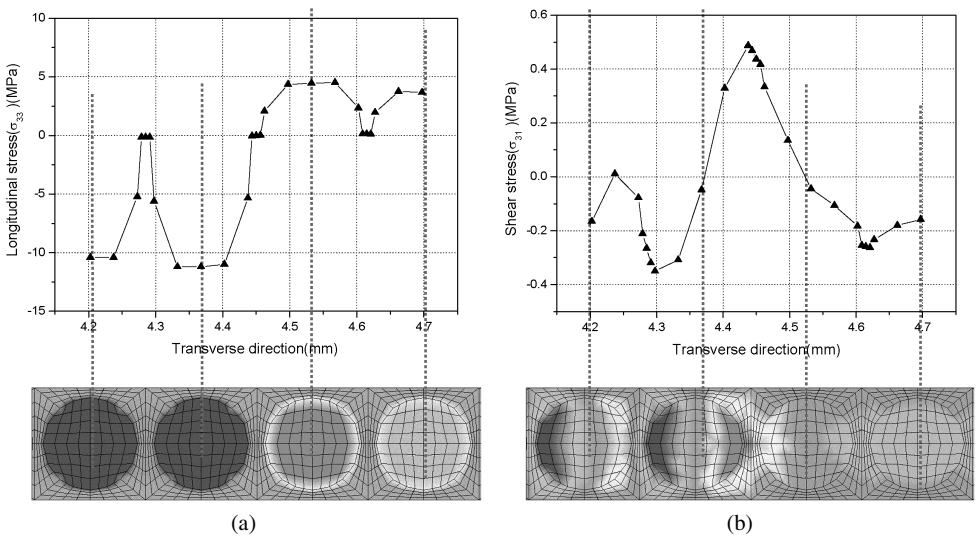

Figure 14. Longitudinal/shear stress distribution in active/inactive transient region: (a) longitudinal stress, (b) shear stress.

defined as transverse actuation divided by longitudinal actuation. As shown in Table 6, the actuation ratio of the laminated AFC shows a good agreement with the experiment. It is almost impossible to measure transverse actuation on the unlaminated AFC actuators, which have no E-glass layers, using strain gages, due to the local buckling of the thin actuators. However, by using the virtual experiment, it can be predicted and proved to be 16% higher than that of the laminated AFC.

Since the piezoelectric fiber elongates when an electric field is applied, shear stresses in the fiber–matrix interface are expected to be relatively large than the other regions in the thickness direction. Figure 14 shows the longitudinal and shear stress distribution along the transverse direction in the active/inactive transient region near the side edge. Four fibers in this region are observed. Two of them in the left hand side are the fibers in the active region and the others are fibers in the inactive region. Fibers in the active region are compressed and those in the inactive region are extended. The magnitude of stress in the active region is higher by two times than that in the inactive region. In the case of shear stress, the maximum value is appeared in active/inactive interface and it is bigger than that in inactive region by approximately 30%.

The second example is a helicopter rotor blade application. AFC is used to control the helicopter rotor blade [21, 22]. Figure 15a shows active fiber composite (AFC) actuators which are embedded in the composite spar laminate at $\pm 45^\circ$ to generate the twist. Figure 15b shows a cross-section of the composite structure highlighting the presence of the AFC plies.

In this part, local stresses in the embedded AFC in the composite structure are observed under the application of electric field. A shown in Fig. 15b, there are 11

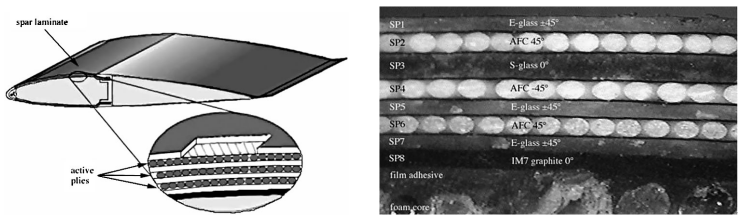

(a) (b)

Figure 15. (a) Integral twist actuation concept [23], (b) a typical cross-section.

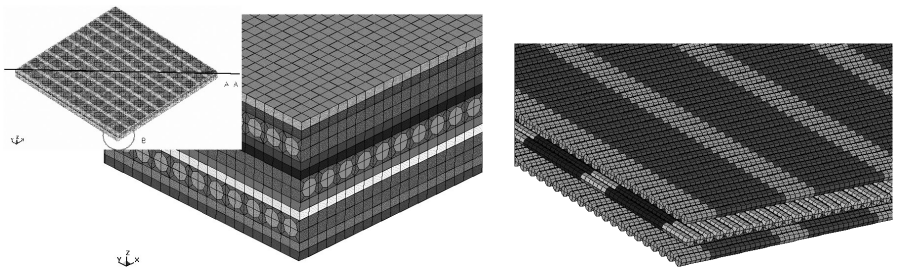

(a) (b)

Figure 16. (a) Magnified view of region B, (b) active/inactive region of active fiber.

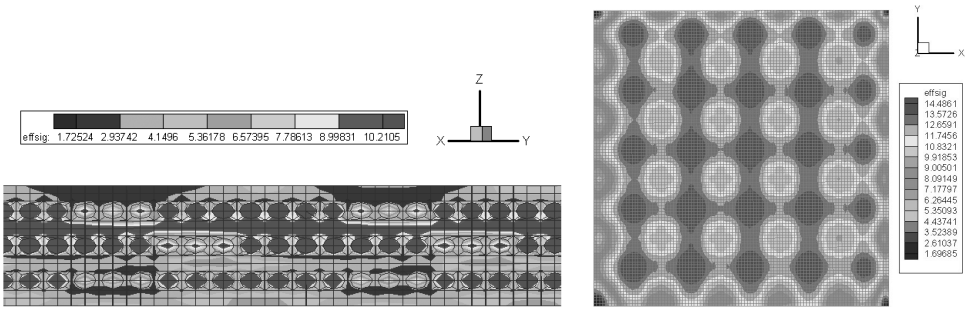

(a) (b)

Figure 17. (a) Stress in the thickness direction, (b) stress in the in-plane direction.

layers on the foam core. In the finite element model, foam core and adhesive are not considered. Instead, fixed boundary conditions are applied on the bottom of the FE model. Figure 16 shows the overall view of the full finite element model. The dimension of the model is 16 mm × 16 mm × 0.98 mm. The total number of nodes is about one million, and the number of degrees of freedom is about three million. Figure 16a shows a magnified view of area B, the corner of the FE model. The number of degrees of freedom of model is about 3 million. In Fig. 16b, the FE mesh of active/inactive region of active fibers is shown. Electrode spacing is chosen as 1 mm with a width of 0.5 mm. The diameter of active fiber is 130 μm and thickness of AFC lamina is 160 μm. The local stress distributions are presented in Fig. 17. Figure 17a shows the stress distribution in thickness direction. Except for

active fibers, stresses are higher in the second polymer layer from the top, which is 0° S-glass layer rather than that of ±45° E-glass layer, which is the first, third and fourth polymer layer from the top. Figure 17b shows the stress distribution in the plane of the second 0° S-glass layer. Locally high stresses are observed along the fiber direction and the electrode pattern.

4.2. Low-Velocity Impact Simulation

It is well known that the transverse stiffness and strength of laminates in the through-the-thickness direction are poor since general laminates have no reinforcement in the thickness direction [25, 26]. This leads to poor transverse impact resistances and interlaminar flexural strength. This gives rise to a local damage that appears as fiber breakage and matrix cracking, and at a global scale as a delamination. They rise near material and geometric discontinuities, highly concentrated loads and at the interface between layers in component materials. Thus, impact damage has been a major issue in the design of laminated composite structures [23]. The strength of composite structures can be significantly reduced by low-velocity impact damage, even if the damage is not detectable by visual inspection. The consequences of impact loading in composite panels are matrix cracking, interlaminar failure and, eventually, fiber breakage for higher impact energies. In the region where damage rises, the interlaminar shear stresses become dominant and the transverse normal stress also important. Insight into the transient dynamic response of impacted composite plates is necessary to establish various failure mechanisms and to improve the performance of composite structures. The effect of low-velocity impact damage of composite structures has been studied extensively by many researchers over the past several decades. The results of these studies show that the strength of composite structures can be significantly reduced by low-velocity impact damage, even if the damage is not detectable by visual inspection.

For these reasons, the effect of low-velocity impact damage on the laminated composite structures has been studied extensively by many researchers over the past several years [24, 25]. Within recent years, some efficient numerical prediction models have also been introduced for studying this problem using 2-D FEM based on the macroscopic homogenized material properties. These approaches were computationally very efficient due to their simplicity for some fundamental problems in this field. However, this 2-D numerical model based on beams or plates may fail to give more realistic prediction information that contains interlaminar stress through the thickness and distribution of micro-stresses inside the constituents such as matrix or fibers. It is limited in describing the behaviors and failure modes that may initiate damage.

To overcome the limitations faced in the 2-D FEM model, many authors have studied these problems based on the layerwise model by Reddy [4] or 3-D FEM analysis using solid elements [26, 27]. The layerwise model is to subdivide the laminate thickness into computational layers, each viewed as an equivalent single layer, then to enforce the displacement and stress contact conditions at interfaces

as constraint conditions. The refinement offered by stacking computational sublayers makes a layerwise model able to capture interlaminar stresses directly from constitutive equations, despite abrupt changes of the material properties across the thickness. However, there are also some apparent limitations in those approaches because they do not consider directly constituent properties inside a layer. In order to accurately capture local stresses in laminated composites, solid finite elements based on mixed variational statement, which have the three displacements and the three interlaminar stresses as the nodal degrees of freedom, have been developed [28], but their uses are limited due to difficulties in applicability to general use. Actually, from a material point of view, most of the present numerical approaches based on the homogenized material properties have been restricted to only rough evaluation of the delamination sizes or prediction of damage, since initial cracking in the ply may occur either in the matrix or at the fiber/matrix interface in the micro-scale.

This paper presents the applicable possibilities of the direct numerical simulation (DNS) for the low-velocity impact phenomena and provides detailed information of their dynamic behaviors in a microscopic aspect. DNS is based on the microscopic approach and the DNS results are compared with the results of the homogenized model, and interlaminar stress distributions with respect to the thickness of plates are compared with the results of the homogenized model.

4.2.1. Metal Matrix Cross-ply Composite Plates (Boron–Aluminum)

The laminated plate $[90_2/0_2/90_2]$ has two interfaces where the direction of fiber is changed (Fig. 18). The fiber volume fraction of the laminates is 47%. The dimension of the laminates plate is $2.4 \times 2.4 \times 0.6$ (mm). For the boundary condition on the DNS model, the nodal displacement constraints are imposed along the 4 edge-lines in the mid-plane of the plate model in order to enable the 4 edge faces

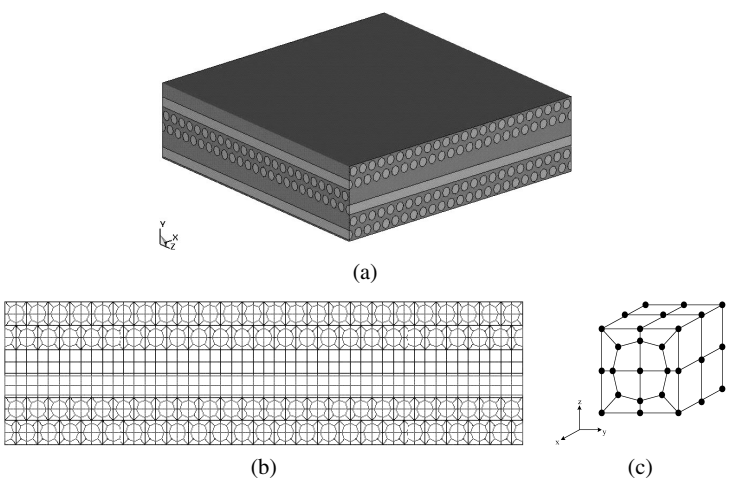

Figure 18. Boron/aluminum cross-ply DNS model: (a) isoparametric view, (b) $x-y$ view and (c) finite element mesh for unit cell.

to rotate on each edge-line of the mid-plane. The impact load is applied at the center of the plate by a rigid ball with the radius of 3.5 mm, which is modeled using 110 triangular shell elements and is assumed to have the mass of 0.43 kg and the initial velocity of 10 m/s in the transverse direction. For contact modeling, the laminated plate was taken as a slave part, whereas the impactor was taken as a master part. Under these definitions, the individual nodes in the laminated plate were constrained not to penetrate the surface of the impactor by the master–slave contact algorithm implemented in LS-DYNA3D. It was assumed that the contact bodies might undergo large motion but their surfaces did not move very much relative to each other.

For comparative study, the DNS model and the homogenized model are investigated and the homogenized model is assumed to be transversely orthotropic and has equivalent material properties. The DNS model and the homogenized model have the same mesh configuration, which is composed of a hexagonal assembled array of unit cells. The response history curves are compared with the results of the homogenized model for displacement and contact force. This investigation was concerned with validation for the DNS model in the macroscopic view. Contact force is calculated by summation of all tractions on the impacted surface layer and no friction is assumed. Displacement is a vertical deflection at the center of the plate where the impact event occurred. As seen in Fig. 19, contact forces and displacements of the DNS model are in a good agreement with the results of the homogenized model in the global sense. Therefore, it can be concluded that the DNS model and the homogenized model have similar global dynamic behaviors of impact. On the other hand, comparison between the DNS model and the homogenized model is shown in Fig. 20. The DNS results present a distinct difference for the spatial von Mises stresses distribution across the y–z cut-section at the center of the plate as compared to the results of the homogenized models. Unlike the homogenized model,

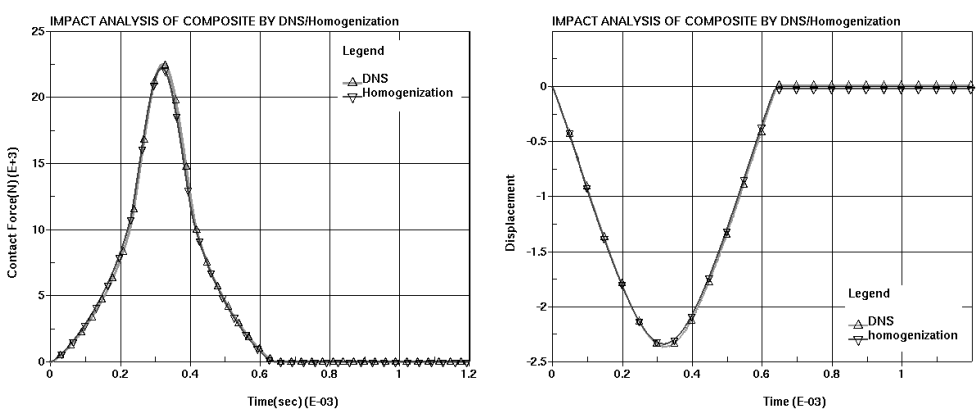

(a) (b)

Figure 19. Comparison between the DNS and the homogenized model for MMC laminates: (a) contact force history, (b) deflection history at the impacted node.

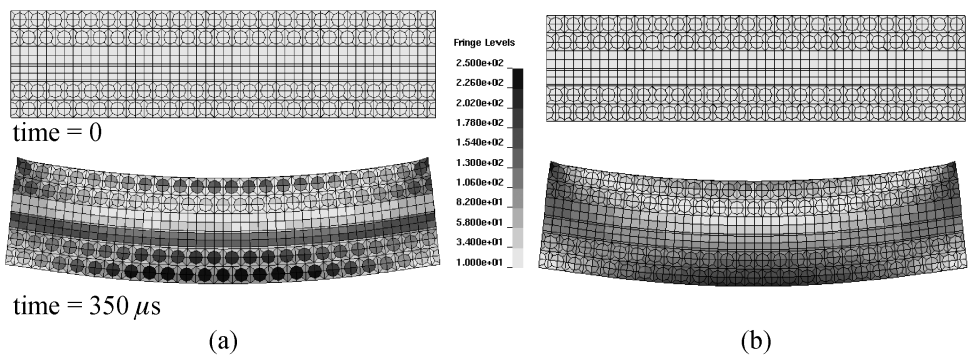

Figure 20. Von Mises stress distribution at the impacted mid-cut section through thickness with time: (a) DNS model, (b) homogenized model.

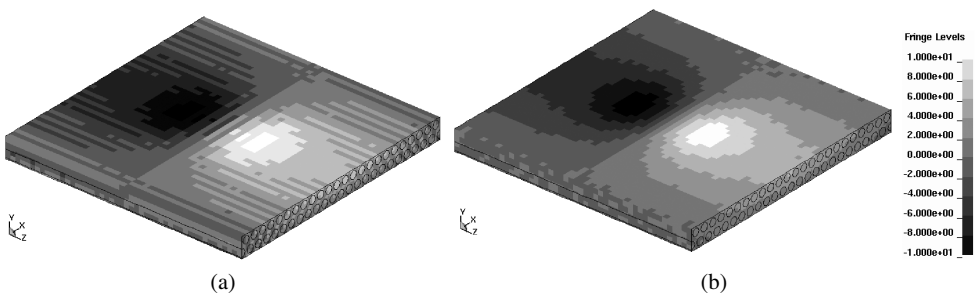

Figure 21. Contours of the interlaminar shear stress σ_{yz} in the lower interface between 0° and 90° layers: (a) DNS model, (b) homogenized model.

the distribution of the DNS model is clearly non-uniform. As one can see, the effects of fiber and matrix are definitely distinguished in the DNS model though they are very similar in the macroscopic view. From Fig. 21 it can be seen that the peanut shape can be produced more similarly in the DNS model from comparison of contours of interlaminar shear stress (σ_{yz}) in the lower interface between 0° and 90° layers. These results agree with the fact that peanut-shaped interlaminar damages caused by low-velocity impact, such as ply crack or delaminations, are generated on the lower interface where fiber angles are changed [29, 30]. Especially, Fig. 22 shows the von Mises stresses variations along ply-thickness direction at the cut section under the impacted area when maximum deformation is occurred. As seen in the graph, a difference of the magnitude of the stresses between two models is larger in the lower layers. These behaviors are significantly influenced by the difference of material properties at the micro-scale and geometrical array distributions of fibers. Especially, the von Mises stress gradient is dramatically changed between lower plies in the DNS model. These steep stress gradients are shown in the interfaces where fiber angles are changed and this effect is not seen in the homogenized model, since the ply micro-structure is smeared. When matrix properties are assumed to be elastoplastic, it is more clearly observed from Fig. 23 in comparison

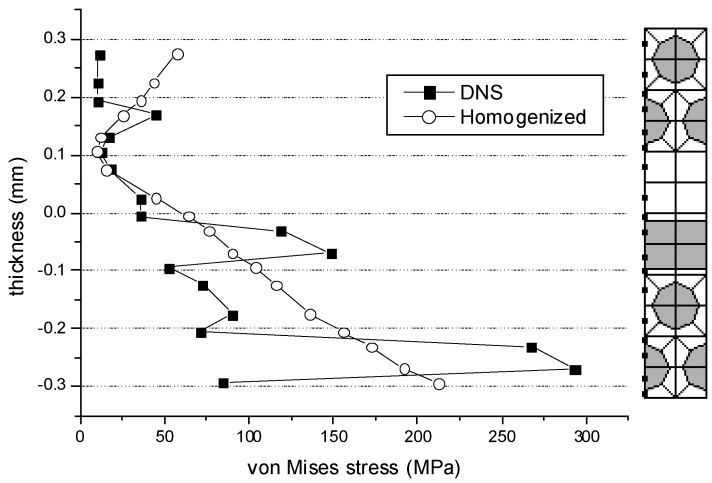

Figure 22. Through-the-thickness variation of von Mises stress for the DNS and homogenized model ($t = 0.35$ ms; max. deformation).

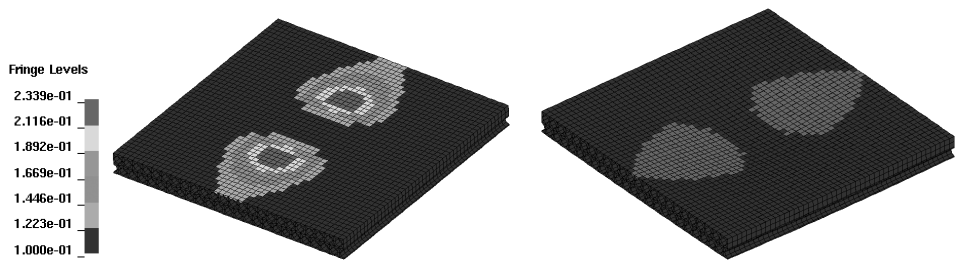

Figure 23. (a) Effective plastic strain distribution and (b) yielded area at lower interface.

with elastic results that peanut-shape delaminations in fibrous composites propagate along the fiber/matrix interfaces adjacent to the resin rich interlaminar region. Therefore, it can be inferred from those results that the DNS model has advantages for describing the local stress states in the inside of materials as compared to the homogenized model.

4.2.2. 3-D Orthogonal Woven Composite Plates

Due to recent advancements in processing techniques, woven composites have been extensively used for impact resistance in applications such as armored vehicles, body armors, and in the aerospace industry as various structural elements. Especially, in the case of 3-D orthogonal woven composites, it is well known that they are more resistant to impact damage, such as delamination and matrix cracking, as compared to unidirectional composites. For the same fiber volume fractions, 3-D orthogonal woven composites show a significant increase in through-the-thickness properties without a comparable reduction in in-plane properties [31]. Even though

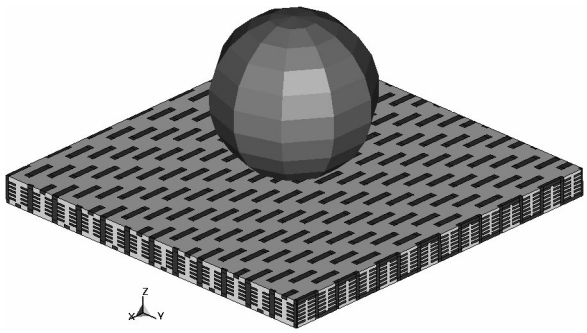

Figure 24. Model of the impact simulation of 3-D woven composite plates.

a number of simplified analytical approaches have been proposed to obtain the dynamic characterization and impact analysis of woven composites, which is based on modified classical laminate theories approach for simplified models of geometry [32, 33], further studies are still necessary considering the information about the real micro-structure of woven composites in as much detail as possible.

The DNS and homogenized models were chosen for these direct numerical impact studies. In this work, the numerical models were defined in terms of the DNS model with isotropic material properties for each constituent, and the homogenized model with orthotropic material properties for the whole system. For impact analysis, we prepared the DNS model by assembling 42 ($7 \times 6 \times 1$) unit structures. The schematic configuration of woven composite plate geometry is shown in Fig. 24. For the present study, a rectangular plate of $38.08 \times 37.68 \times 2.79$ (mm) thickness was considered. The total degree of freedom of this model is 1.56 million. The supported boundary condition was 4-edge clamped. A spherical impactor with radius 8.0 mm was considered to be rigid and its initial velocity was 5 m/s.

Global response plots, displacements and contact force histories of two models are presented in Fig. 25a and 25b, respectively. It is observed from Fig. 25, that the values obtained using the DNS model are found to be in good agreement with those obtained by the homogenized model. Hence, it is concluded that the DNS model considering the micro-structures of constituents has effective dynamic properties corresponding to the homogenized model in spite of the differences of material properties in the microscopic sense. Additionally, it can be seen from Fig. 25b that the contact condition was well applied and multiple contacts occurred for both DNS and homogenized models. Figure 26 depicts the von Mises stress distribution on the surface, which directly impacted by the impactor at the time when the maximum contact force occurs. From Fig. 27, it can be shown that stress values are high in the vicinity of the impacted point and a relatively high stress values are shown in the warp yarns rather than neighboring matrix area.

In addition, impact behaviors of 3-D woven composites that have non-uniform internal geometries of yarns are also investigated using the DNS models (Fig. 27). The central deflections and contact force histories of each case are shown in Fig. 28.

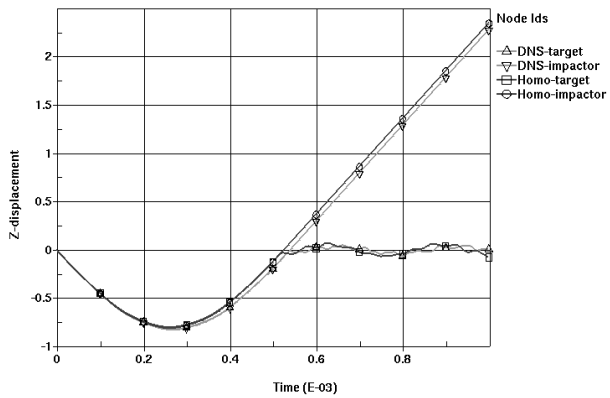

(a)

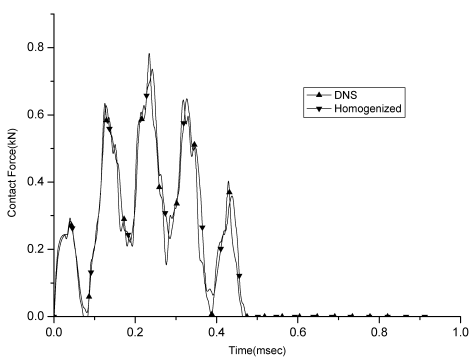

(b)

Figure 25. (a) Transverse displacements history of impactor and target (mm), (b) contact force history (N).

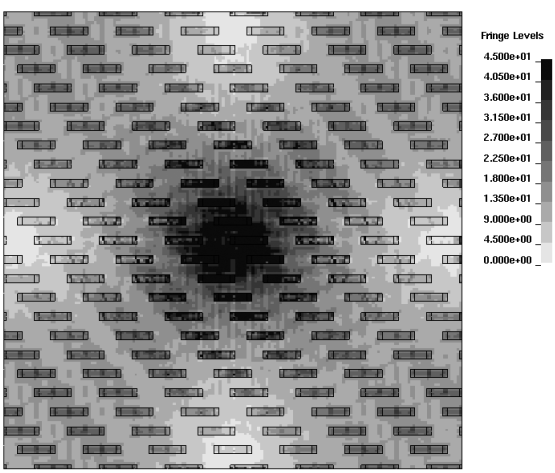

Figure 26. Von Mises stress distribution of 3-D orthogonal woven composites at $t = 0.26$ ms.

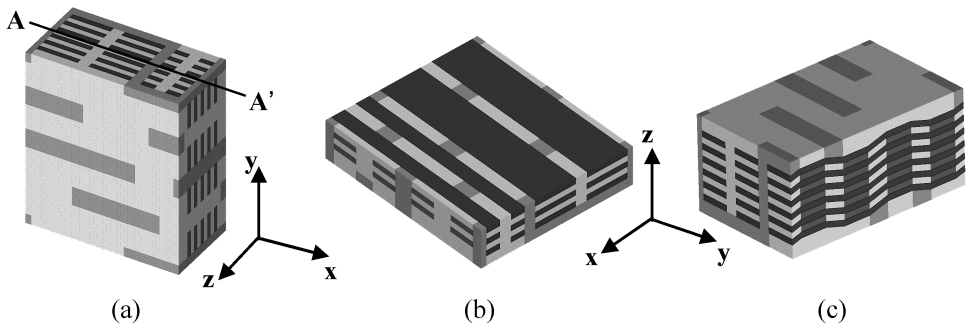

Figure 27. The schematic drawing of unit structure of tow spacing and waviness model.

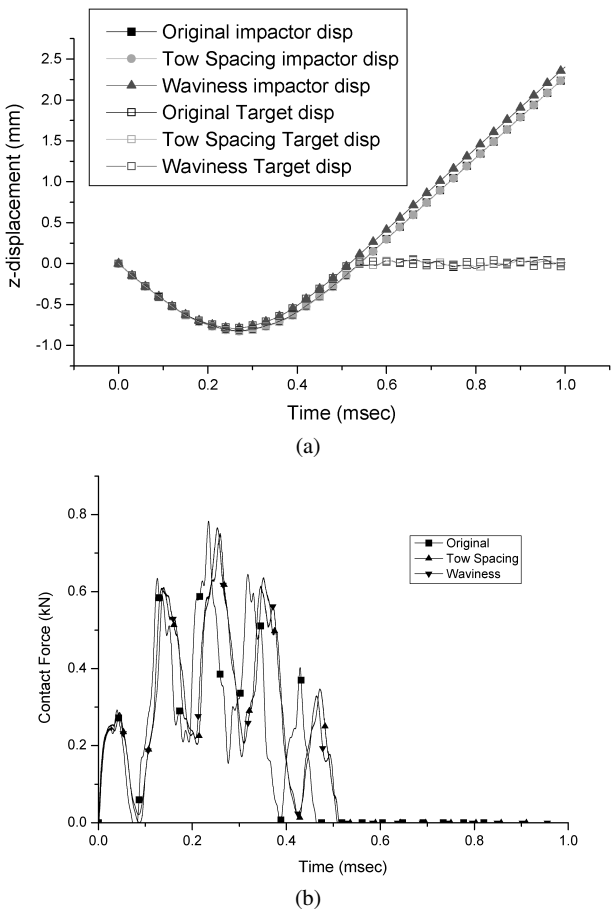

Figure 28. (a) Transverse displacements of impactor and target in z-direction (mm), (b) contact force history (N).

The values of transverse central deflections are relatively similar with all the cases; but there are some differences in the contact force histories. The waviness model

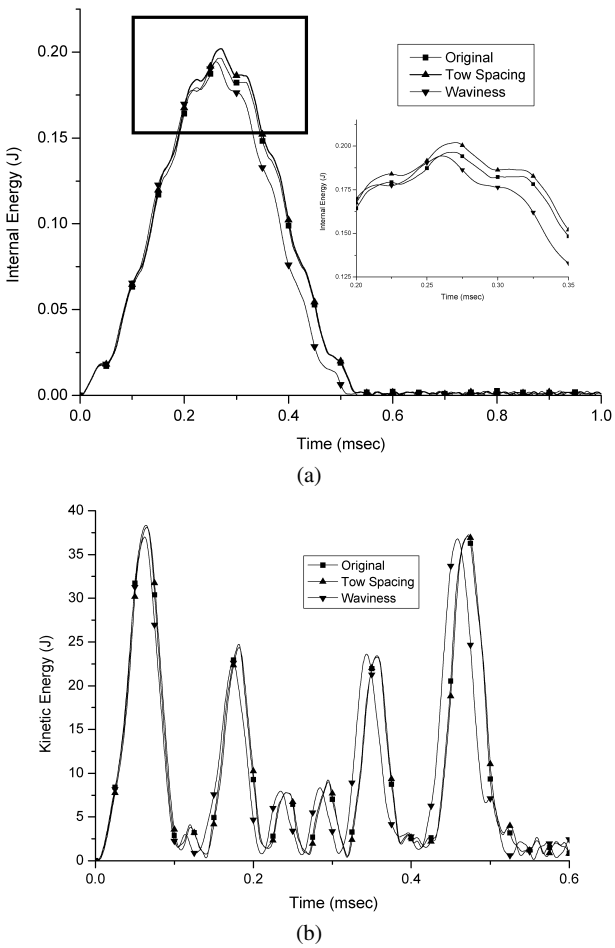

Figure 29. (a) Internal energy history, (b) kinetic energy history.

and tow spacing model have a little more delayed contact duration time as compared to the original model though the peak contact force is nearly the same for all cases. Corresponding time histories of internal and kinetic energy of each model are presented in Fig. 29. During the process that the kinetic energy of the impactor is transformed into the internal and kinetic energy of the target structure, the waviness model takes a relatively lower transferred internal energy. Moreover, the phase of the kinetic energy of only the waviness model is time-shifted to the left allowing that the peak values of the kinetic energy show only little change. From these results, these are because woven composites with waviness of fillers have reduced stiffness caused by waviness and geometrical irregularities due to waviness are more influential in loss of impact resistance than tow spacing irregularities.

5. Multi-scale Impact Simulation of Composite Plates

Composite materials are inherently heterogeneous from the microscopic view. From a macroscopic view, material properties of a composite are derived from a weighted average of the constituent materials, such as fiber and matrix. But impact damages on composite materials occur by complex mechanisms that may be dependent on the microscopic geometry information inside of material specimens and interactions between constituents at a micro-scale level. The multi-scale models developed in this study are presented in order to describe the impact phenomena at different characteristic length scale, which is effective for accurate impact analysis. As suggested in the introductory part, a realistic model of composite geometry is needed in order to obtain a reliable estimate of both the local and overall response of real composites under certain loading conditions. However, such a model might be quite complex, leading to an enormous computational cost. The computational feasibility, on the other hand, calls for rather simple models usually specified in terms of homogenized material properties. For these reasons, the conventional approaches to numerical impact analysis have so far used the simple model with the homogenized anisotropic material properties regardless of microscopic geometry of constituents.

Various multi-scale computational techniques have been presented recently. Most of them were based on the asymptotic homogenization theory using asymptotic expansions of displacement, strain and stress fields, which has been used as a popular tool for analyzing multiple scale response in [34, 35]. Multiple scale computational analysis of reinforced composites, utilizing this method, has been conducted by Fish and Shek [36], Tamma and Chung [37], Ghosh *et al.* [38] and others. Most of the homogenization models make assumptions of periodic representative volume elements (RVE) in the micro-structure and of uniformity in the macroscopic field variables. However, it is reported that macroscopic uniformity is not an appropriate assumption, for example, in regions of high gradients like free edges, interfaces, material discontinuities or in regions of localized evolving damage [39]. Even for geometrically periodic micro-structures, periodicity assumptions may not be appropriate when deformation or damage is localized. Hierarchical multi-scale modeling, differentiating between regions requiring different resolutions, is becoming an increasingly more effective tool for modeling deformation and damage in heterogeneous materials. Substructuring in these models enables pure macroscopic analysis in some parts of the domain using homogenized or effective material properties and zooming in for local or microscopic modeling at a different scale in other regions of the domain. Such shortcomings for composite material modeling have been discussed for modeling various heterogeneous problems by Pagano and Rybicki [40] and by Oden and coworkers [41].

In the present work, multi-scale models are developed based on DNS concepts that can be designed for the microscopic approach to a low-velocity impact problem. They contain the macro/micro-scale parts for the cross-ply laminate plate. In the macro-scale parts, composite materials are considered as homogenized anisotropic materials and anisotropic constitutive equations are directly adopted.

The lamina's homogenized mechanical properties are obtained by material characterization directly using the mechanical properties of constituents. In the micro-scale part, since composite materials are regarded as a mixture of different isotropic materials, separate discretization of fiber and matrix is required to describe the micro behavior of the constituents. Especially, impact-induced damage, like all physical phenomena, exists in general on different scales and appears differently depending on the scale of observation. The microscopic and local behavior is determined by interactions between particles and influences macroscopic properties of the considered system. We adopt the DNS concepts in the microscopic modeling and employ the tied interface constraints that are provided by LS-DYNA3D [42] as interfaces connecting micro- and macro-model.

5.1. Boron/Epoxy Cross-ply and 3-D Orthogonal Woven Composite Plates

The composite plate studied here for multi-scale DNS is a boron/5505 epoxy laminate $[0_2/90_6/0_2]$ and 3-D orthogonal woven composites. The laminates DNS model has 6,574,500 d.o.f.s and the woven composite DNS model has 10,809,072 d.o.f.s. Their material properties are presented in Table 1 and Table 3 above. Each multi-scale DNS model for the plate is composed of the micro-scale and macro-scale finite element model, which are presented together in Fig. 30 for boron/epoxy laminates and 3-D orthogonal woven composite plates.

In order to show the successful application of the tied-interface constraint used in the DNS model, Fig. 31 shows that contours of z-direction displacements of boron/epoxy laminates change with time. It is observed that continuity of displacement fields is preserved at the boundary of the micro/macro-model in the present multi-scale model. Figure 32 depicts von Mises stress spatial distribution in the lower fiber angle-changed interface (x–y cut-section) of laminate model at the time when the maximum contact force is reached. Even though only von Mises stress distribution is considered, the shape is similar with the peanut shape which is encountered in the real experimental results [31]. The history of von Mises stresses

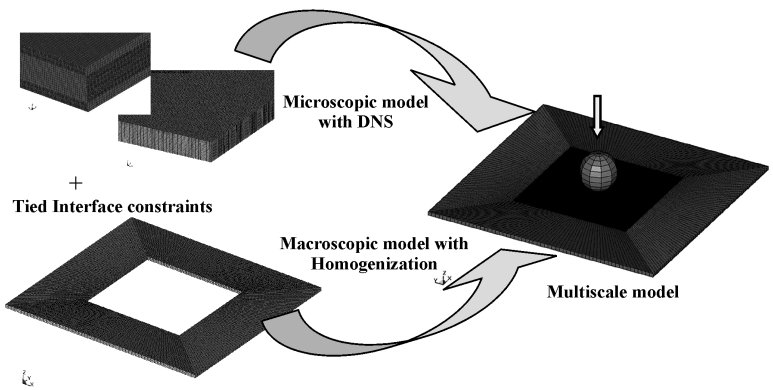

Figure 30. Multi-scale model of boron/epoxy cross-ply laminates and 3-D orthogonal woven composites.

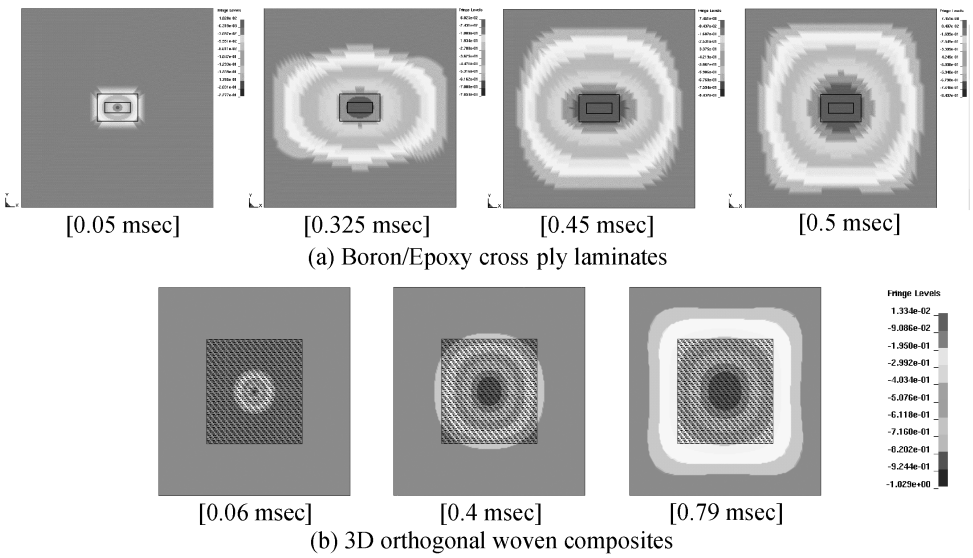

Figure 31. Spatial contours of displacements on the top surface with time change.

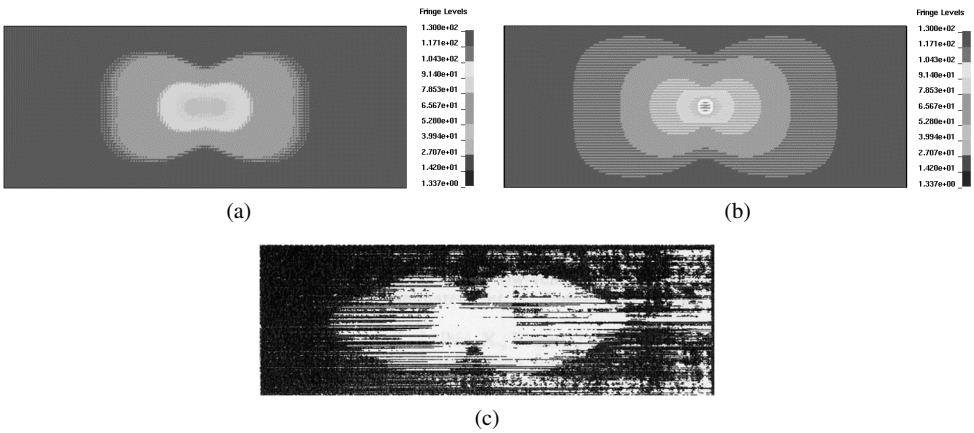

Figure 32. Calculated effective stress (von Mises) distribution: (a) upper interfaces [0/90], (b) lower interfaces [90/0] and (c) experimental result [6].

through-the-thickness at the y–z cut-section is plotted in Figs 33 and 34 in order to investigate near the upper interface and lower interface. The stresses are extracted from the matrix and Fig. 33 represents the stress histories of the matrix in the plies near the upper interface [0°/90°] and Fig. 34 for the lower interfaces [90°/0°]. From these figures, it is noticed that relatively high stresses occurs in the area of the directly impacted surface layer (Area A) and the layer beneath the lower interface (Area D). Especially, as mentioned above, higher stresses appear in the lower interface than in the upper interface. This detailed information inside the matrix cannot be obtained from the homogenized model.

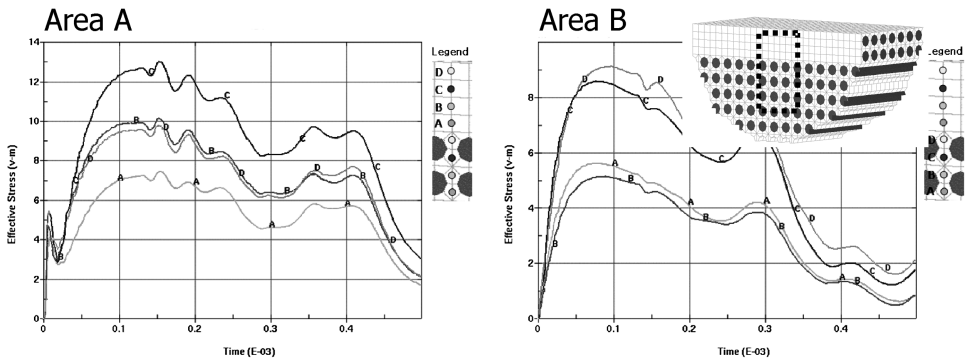

(a) (b)

Figure 33. Von Mises stress time history at the constituents' level — upper [0/90] boundary.

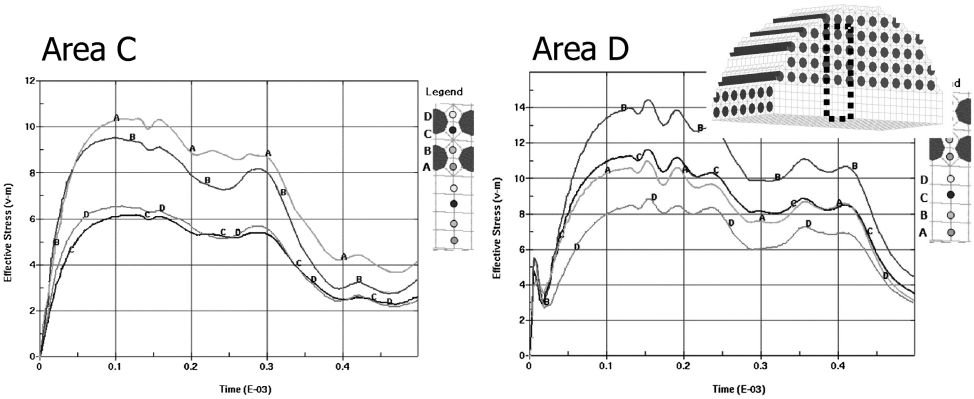

(a) (b)

Figure 34. Von Mises stress time history at the constituents' level — lower [90/0] boundary.

Figures 35–37 are related to the multi-scale DNS analysis of 3-D orthogonal woven composite plates. Figure 35 shows the internal and kinetic energy distribution of each constituent during impact. It is impossible to obtain the individual information of constituents using the conventional approach based on homogenization. It is found that the matrix takes the greatest portion of the internal energy by deformation out of the total mechanical energy which the impactor had initially. Also, from a view of kinetic energy, matrix and stuffer yarn have a larger portion of kinetic energy than any other components. From these results, it can be concluded that the matrix plays a relatively major role in absorbing internal and kinetic energy due to impact. Warp weaver seems to make relatively a little contribution to absorption of energy in Fig. 35. However, Fig. 35 shows the effect of warp weaver which makes the transverse stiffness higher. In Fig. 36, when we compare the central deflection and internal energy histories of the two models with or without warp weaver, the model without warp weaver has larger deflection and internal energy than the model with warp weaver. These results indicate that the woven composite

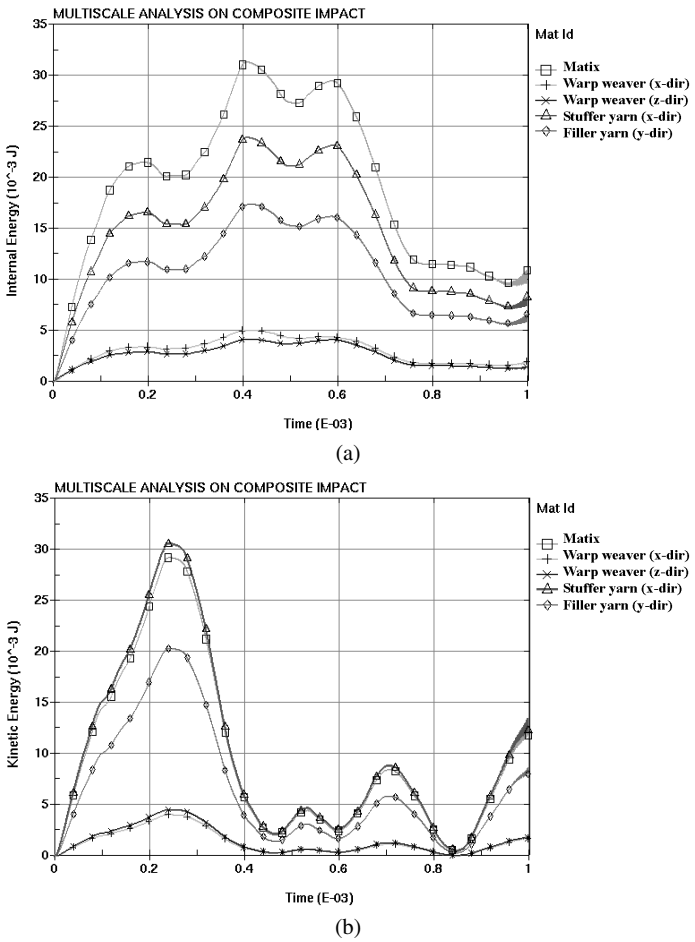

Figure 35. (a) Internal energy history, (b) kinetic energy history of multi-scale model.

model with warp weaver is more resistant to impact compared to the model without warp weaver. Figure 37 shows the effective von Mises stress is mainly transmitted through stuffer and filler yarns rather than matrix, and depicts the transmission process of effective stresses in the region of the micro- and macro-model simultaneously. Herein, the domain presented in Fig. 37 covers a quarter model and the continuity of the values of the effective stresses during the transmission process can be observed easily at the tied interfaces of the micro/macro-model.

6. Conclusions

A micro-mechanical DNS model for some composite materials, such as MMC, AFC, and 3-D woven composites has been presented. The DNS model is based on a repeated unit structure which includes the information about the real microstructure of composite materials in as much detail as possible. The DNS model is

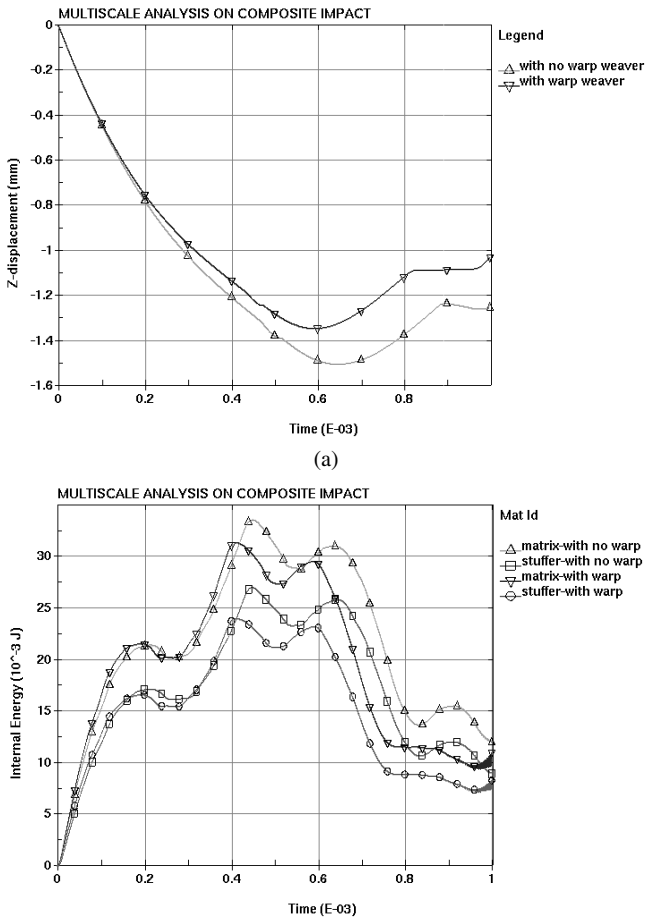

Figure 36. The effect of warp weaver: (a) central deflection, (b) internal energy.

developed considering geometry, impact condition and multi-scale. The proposed methodology is based on the microscopic approach and finite element method, and extends the domain of microscopic analysis to real structures. Transient impact response analysis is conducted using the DNS model with accurate material properties that are determined and verified from material characterization. Not only are the global impact responses presented about the contact force and central deflections, but also the local impact responses are presented about the distributions of inplane and interlaminar stresses and propagation inside the materials at the constituent level. The comparison with the homogenized model makes it clear that the DNS model is able to describe the stresses near the area where the steep stress gradient occurs, while the classical homogenized approach is not able to describe those. DNS can describe the spatial distribution of interlaminar stresses at the micro-level, which is responsible for interlaminar damage such as delamination. In addition, in

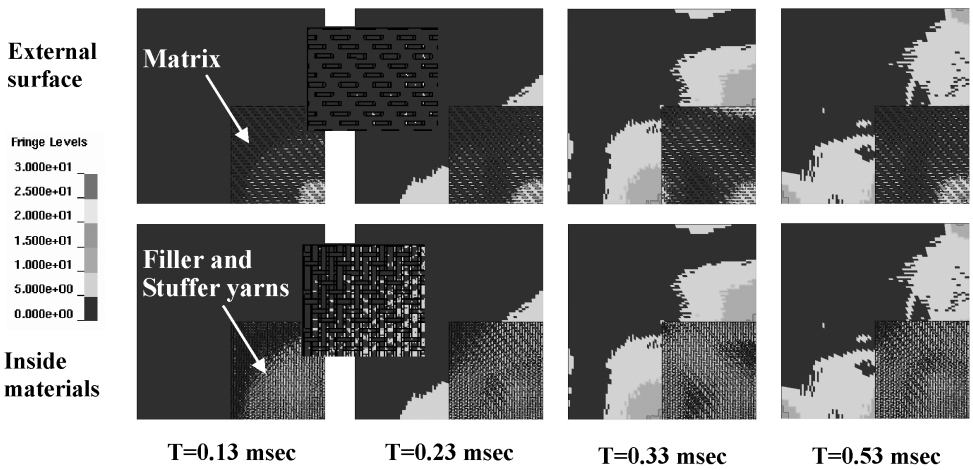

Figure 37. Transmission of the von Mises stress of yarn and matrix inside materials.

order to enhance the effectiveness of DNS analysis, the multi-scale model based on the DNS approach is developed as a real structure size using the tied interface constraints and the results related to global and local behaviors are presented.

Also, a multi-scale model is presented in this paper in order to enhance the effectiveness of the DNS approach. In this multi-scale study, the scales being considered are the micro-scale at the directly impacted area and the macro-scale in the other area. Instead of the full microscopic modeling of the whole composite structures, in different scales, complex phenomena, such as the interaction between fiber and matrix, can be effectively described.

DNS modeling of composite materials has proven to be a successful and valuable tool of investigation. The applicability of materials theory to almost any established and newly emerging topic of materials science promises that it will play an increasingly guiding, stimulating and visionary role in the search for composite materials. These technologies promise to be orders of magnitude faster than conventional electronic computers and will revolute DNS at all levels. Advances in computing power in the next decade will significantly expand the regime of applicability for many of these methods.

Acknowledgements

The research was supported by National Research Program, R0A-2006-000-10178. The authors are grateful to Korea Science Foundation and Ministry of Education, Science and Technology for their support.

References

1. R. M. Jones, *Mechanics of Composite Materials*. McGraw-Hill Book Company, New York, USA (1975).

2. R. F. Gibson, *Principles of Composite Material Mechanics*. McGraw-Hill Book Company, New York, USA (1994).
3. N. J. Pagano and F. G. Yuan, The significance of effective modulus theory (homogenization) in composite laminate mechanics, *Compos. Sci. Technol.* **60**, 2471–2488 (2000).
4. J. N. Reddy, *Mechanics of Laminated Composite Plates: Theory and Analysis*. CRC Press, Boca Raton, FL, USA (1997).
5. J. Aboudi, *Mechanics of Composite Materials: A Unified Micro-Mechanical Approach*. Elsevier, New York, USA (1991).
6. C. T. Sun and R. S. Vaidya, Prediction of composite properties from a representative volume element, *Compos. Sci. Technol.* **56**, 171–179 (1996).
7. Y. W. Kwon and J. M. Berner, Micromechanics model for damage and failure analysis of laminated fibrous composites, *Engng Fract. Mech.* **52**, 231–242 (1995).
8. S. J. Kim, J. Y. Cho and J. H. Kim, Finite element modeling and analysis of composite structures, in: *Proc. 1st Korea–US Workshop on Compos. Mater.*, Seoul, Korea (1998).
9. J. Y. Cho, J. H. Kim, C. S. Lee and S. J. Kim, Determination of composite material constants by direct numerical simulation, in: *Proc. 12th Intl Conf. Compos. Mater.*, Paris, France (1999).
10. S. J. Kim, C. S. Lee, H. J. Yeo, J. H. Kim and J. Y. Cho, Direct numerical simulation of composite structures, *J. Compos. Mater.* **36**, 2765–2785 (2002).
11. J. W. Park and S. H. Park, Optimal blade system design of a new concept VTOL vehicle using the departmental computing grid system, in: *Supercomputing Conference 2004*, S. Hwang, J. J. Moon, Y. Yoon and S. J. Kim, Pittsburgh, PA, USA (2004).
12. D. Kenaga, J. F. Doyle and C. T. Sun, The characterization of boron aluminum in the nonlinear range as an orthotropic elastic plastic material, *J. Compos. Mater.* **21**, 516–531 (1987).
13. D. Fang, H. Qi and S. Tu, Elastic and plastic properties of metal-metal composites: geometrical effects of particles, *Comput. Mater. Sci.* **6**, 303–309 (1996).
14. M. M. Aghdam, D. J. Smith and M. J. Pavier, Finite element micromechanical modeling of yield and collapse behaviour of metal matrix composites, *J. Mech. Phys. Solids* **48**, 499–528 (2000).
15. T. H. Yoon, S. H. Paik, S. J. Shin and S. J. Kim, Computational material characterization of active fiber composite, in: *15th Intl Conf. Adaptive Struct. Technol.*, Atlantic Oakes By-the-Sea, Bar Harbor, Maine, USA (2004).
16. V. Wickramasinghe and N. Hagood, Material characterization of active fiber composite actuators for active twist helicopter rotor blade applications, in: *41st AIAA/ASME/ASCE/AHS/ASC, Structures, Structural Dynamics, and Materials Conference and Exhibit*, Atlanta, GA, USA (2000).
17. C. C. Chamis, Simplified composite micromechanics equations for hygral, thermal, and mechanical properties, *SAMPE Quarterly* **15**, 14–23 (1984).
18. P. Tan, L. Tong and G. P. Steven, Modeling approaches for 3D orthogonal woven composites, *J. Reinf. Plast. Compos.* **17**, 545–577 (1998).
19. S. J. Kim, C. S. Lee and H. Shin, Virtual experimental characterization of 3D orthogonal woven composite materials, in: *42nd AIAA/ASME/ASCE/AHS/ASC Structures, Structural Dynamics, and Materials Conference and Exhibit*, Sheraton Seattle Hotel and Towers, Seattle, WA, USA (2001).
20. P. Tan, L. Tong, G. P. Steven and T. Ishikawa, Behavior of 3D orthogonal woven CFRP composites. Part I. Experimental investigation, *Composites, Part A: Appl. Sci. Manuf.* **31**, 259–271 (2000).
21. J. P. Rodgers and N. W. Hagood, Hover testing of a 1/6th mach-scale CH-47D blade with integral twist actuation, in: *9th ICAST*, Cambridge, MA, USA (1998).
22. H. B. Strock, M. R. Pascucci, M. V. Parish, A. A. Bent and T. R. Shrout, Active PZT fibers, a commercial production process, in: *SPIE's 6th Ann. Intl Sympos. on Smart Structures and Materials*, Newport Beach, USA (1999).

23. S. Abrate, Impact on laminated composite materials, *Appl. Mech. Rev.* **44**, 155–190 (1991).
24. W. J. Cantwell and J. Morton, The impact resistance of composite materials — a review, *Composites* **22**, 347–362 (1991).
25. M. O. W. Richardson and M. J. Wisheart, Review of low-velocity impact properties of composite materials, *Composites, Part A: Appl. Sci. Manuf.* **27**, 1123–1131 (1996).
26. F. Collombet, X. Lalbin and J. L. Lataillade, Impact behavior of laminated composites: physical basis for finite element analysis, *Compos. Sci. Technol.* **58**, 463–478 (1998).
27. C. F. Li, N. Hu, Y. J. Yin, H. Sekine and H. Fukunaga, Low-velocity impact-induced damage of continuous fiber-reinforced composite laminates. Part I. An FEM numerical model, *Composites: Part A* **33**, 1055–1062 (2002).
28. J. P. Hou, N. Petrinic, C. Ruiz and S. R. Hallett, Prediction of impact damage in composite plates, *Compos. Sci. Technol.* **60**, 273–281 (2000).
29. H. Y. Choi and F. K. Chang, A model for predicting damage in graphite/epoxy laminated composites resulting from low-velocity point impact, *J. Compos. Mater.* **26**, 2134–2169 (1992).
30. H. Y. Choi, H. Y. Wu and F. K. Chang, A new approach toward understanding damage mechanisms and mechanics of laminated composites due to low-velocity impact. Part II. Analysis, *J. Compos. Mater.* **25**, 1012–1038 (1991).
31. M. V. Hosur, M. R. Karim and S. Jeelani, Experimental investigations on the response of stitched/unstitched woven S2-glass/SC15 epoxy composites under single and repeated low-velocity impact loading, *Compos. Struct.* **62**, 89–102 (2004).
32. N. K. Naik, Y. C. Sekher and S. Meduri, Damage in woven-fabric composites subjected to low-velocity impact, *Compos. Sci. Technol.* **60**, 731–744 (2000).
33. J. N. Baucom and M. A. Zikry, Low-velocity impact damage progression in woven E-glass composite systems, *Composites: Part A* **36**, 658–664 (2005).
34. A. Benssousan, J. L. Lions and G. Papanicoulau, *Asymptotic Analysis for Periodic Structures*. North Holland, Amsterdam, The Netherlands (1978).
35. J. L. Lions, On some homogenization problems, *Zeitschrift fur Angewandte Mathematik und Mechanik* **62**, 251–262 (1980).
36. J. Fish and K. Shek, Multiscale analysis of composite materials and structures, *Compos. Sci. Technol.* **60**, 2547–2556 (2000).
37. K. K. Tamma and P. W. Chung, Woven fabric composites: developments in engineering bounds, homogenization and applications, *Intl J. Numer. Method Engng* **45**, 1757–1790 (1999).
38. S. Ghosh, K. Lee and S. Moorthy, A multi-level computational model for multi-scale damage analysis in composite and porous materials, *Intl J. Solid Struct.* **38**, 2335–2385 (2001).
39. P. Raghavan and S. Ghosh, Concurrent multi-scale analysis of elastic composites by a multi-level computational model, *Comput. Methods Appl. Mech. Engng* **193**, 497–538 (2004).
40. N. J. Pagano and E. F. Rybicki, On the significance of effective modulus solutions for fibrous composites, *J. Compos. Mater.* **8**, 214–218 (1974).
41. T. I. Zohdi, J. T. Oden and G. J. Rodin, Hierarchical modeling of heterogeneous solids, *Comput. Methods Appl. Mech. Engng* **172**, 3–25 (1999).
42. J. O. Hallquist, *LS-DYNA3D Theoretical Manual*. Livermore Software Technology Corporation, Livermore, CA (1998).